Signal Denoising of MEMS vector hydrophone based on optimized VMD, compressed sensing, and Wavelet threshold

HONGPING HU, NANA ZOU, YANPING BAI
School of Science, North University of China,
Taiyuan, Shanxi, 030051
CHINA

Abstract: With the noise in underwater acoustic signal extracted from ocean background, the denoising algorithm based on the Variational Mode Decomposition (VMD) optimized by improved Grasshopper Optimization Algorithm (IGOA), the compressed sensing (CS) and wavelet threshold (WT) is proposed in this paper, named by IGOA-VMD-CS-WT, where VMD optimized by IGOA is utilized to perform sign composition and the obtained Intrinsic Mode Functions (IMF) are divided into effective components and noise components using cross-correlation coefficient of each IMF. CS is performed on sparse representation of noise components and the obtained sparse coefficients are processed with WT for the filters. The effective components and the denoised components are reconstructed to the denoised signal by the Orthogonal Matching Pursuit. The experiments show that IGOA-VMD-CS-WT has the highest signal-to-noise ratios and the least root mean square errors under different noise levels and has the better denoising effect on the denoising of the actual data.

Keywords: Grasshopper Optimisation Algorithm, Variational Mode Decomposition, Compressed Sensing, Wavelet Threshold, Signal Denoising

Received: May 13, 2021. Revised: July 23, 2022. Accepted: August 17, 2022. Published: September 19, 2022.

1. Introduction

IN underwater acoustics, vector hydrophone with its convenience for submarine detection has succeeded in attracting wide attention. According to the principle of the fish lateral organs and the acoustic theory of cylinder, MEMS vector hydrophone performs the detection of underwater signal through the stimulation perception of varistor [1-2]. With small size, high sensitivity, low-frequency detection, and other excellent performance, there exist many kinds of hydrophones and their application [3-4]. However, owing to the complicated underwater acoustic environment in the ocean or lake, there exists inevitably noise and distortion in the signal collected by MEMS vector hydrophone, which affects the subsequent signal detection, directional positioning, classification, and recognition. Therefore, it is essential to adopt the denoising algorithms for performing signal denoising to facilitate the smooth development of the follow-up work.

There are rich denoising algorithms, such as Fourier transform(FT) [5], wavelet transform (WT)[6], singular spectrum decomposition(SSD)[7], Empirical Mode Decomposition (EMD)[8] and their improvements, Variational Mode Decomposition(VMD)[9] and the joint denoising algorithms. Generally speaking, there exist certain denoised effects obtained by these algorithms, but these algorithms have shortcomings, which leads to the careful consideration. FT can show the relationship between the time domain and frequency domain and can be applied to the analysis and processing of stationary signals, but it cannot reflect the characteristics of specific time signals. WT is more effective and practical, and for the signal denoising and the image denoising, WT has the better-denoised results and is more suitable for the unstable signal denoising. The principle components in SSD need to be selected. Self-adaptability is one of the advantages of EMD and the decomposed modal functions obtained by EMD are screened out by their properties. And EMD is applied to non-linear and non-stationary signals and achieves a better denoising effect. However, there are shortcomings of EMD, such as the lack of a strictly mathematical basis, low efficiency, and mode aliasing, which lead to the limitations to a certain extent in its applications and development. VMD proposed in 2013 is a self-adaptive, non-recursive signal decomposition algorithm, which performs partitioning the signal in the frequency domain to achieve effective separation. Different from EMD, VMD has a very strong mathematical foundation, better noise robustness, and higher operational efficiency. But the parameters of VMD are set up in advance. At present, a large number of experimental researches show that a hybrid denoising algorithm has better performance than a single denoising algorithm. For example, VMD is combined with the nonlinear wavelet threshold (NWT) to establish the joint denoising method VMD-NWT for performing denoising and baseline drift removal [10].

Recently, there are more and more metaheuristic algorithms which are divided into two types[11,12]: single

solution-based and population-based, where there is only one solution during the optimization phase in the former type and there are *N* solutions in every iteration during the optimization phase in the latter type. Especially, in the population-based metaheuristic algorithms, Harris Hawks Optimizer[12] is obtained from the cooperative behavior and chasing style of Harris' haws in nature called surprise pounce; the genetic algorithm [13,14] mimics the Darwinian theory of evolution; the particle swarm optimization(PSO)[15] mimics the birds flocking behaviors; Grasshopper Optimization Algorithm(GOA)[16] mimics the behavior of grasshopper swarms in nature for solving optimization problems.

Generally, the parameters of VMD are the number of Intrinsic Mode Functions (IMFs) and the penalty factor. The suitable parameters make the denoising results more effective. The births of metaheuristic algorithms support the opportunities for the parameters of VMD. In the reference [17], the parameters of VMD are optimized by the whale optimization algorithm (WOA), the power spectrum entropy (PSE) is taken to be the fitness function of WOA, and thus the whale-optimized VMD and correlation coefficient (CC) are combined to propose a denoising and baseline drift removal algorithm. In the reference [18], a hybrid algorithm of Multi-Verse Optimizer and PSO is proposed to optimize the parameters of VMD and then is combined with WT denoising and CC judgment to perform the signal denoising of MEMS vector hydrophone.

The definition of Compressed sensing (CS) is that if a high-dimensional signal is compressible or sparse in a certain transform domain, it is mapped into a low dimensional space by a measurement matrix unrelated to the transform basis, and then the original signal is reconstructed from the small number of projection measurements with high probability by solving an optimization problem. The combinations of CS and other algorithms have been widely used in the medical, earthquake, image optimization, and other fields, such as the combination of EMD, CS, and WT for denoising microseismic signals [19], and a method of noise attenuation of the weak seismic signal based on CS and CEEMD [20], the hybrid algorithm based on improved SSA and CS for lidar signal denoising [21].

In this paper, the improved GOA (IGOA) is proposed to be applied to optimize the parameters of VMD for performing sign composition and the obtained IMFs are divided into the effective components and noise components according to the cross-correlation coefficient of each IMF. And CS is used to perform sparse representation of the noise components and the obtained sparse coefficients are processed by being combined with WT for the filters. Then the effective components and the denoised components are reconstructed to the denoised signal. Thus the denoising algorithm based on VMD optimized by IGOA, CS, and WT is proposed in this paper, named IGOA-VMD-CS-WT. The simulation experiments show that the proposed denoising algorithm IGOA-VMD-CS-WT in this paper has the highest signal-to-noise ratios and the least root mean square errors for the simulated signals under different noise levels, superior to the other compared denoising algorithms. Finally, the proposed denoising algorithm IGOA-VMD-CS-WT is applied to perform the denoising of the actual data.

The remaining paper is organized as follows. Section 1 is the introduction. Section 2 gives a brief description of the relevant principles and methods, and the proposed method IGOA-VMD-CS-WT in Section 3 is described in detail. Experiment results for denoising are given in Section 4 for the simulated signal and the Fenji lake trial data obtained from the North University of China. Section 5 is the conclusion.

2. Basic Principles

2.1 Grasshopper Optimization Algorithm

Because VMD cannot be decomposed adaptively, it needs to set parameters in advance, so this paper optimizes its parameters by GOA.

GOA[16] proposed in 2017 simulates the characteristics of small-scale movement during the locust larvae period and random large-scale movement during the adult period, which constitutes the local development and global exploration process of the GOA algorithm. Without considering the gravity factor and assuming that the wind direction always points to the target location, the behavior of the locust swarm can be represented by the following mathematical model:

$$X_i^d = c\sum_{j=1,j\neq i}^{N} c\frac{ub_d - lb_d}{2} s\left(\left|x_j^d - x_i^d\right|\right)\frac{x_j - x_i}{d_{ij}} + \hat{T}_d, \qquad (1)$$

where X_i^d represents the position of the *i*th grasshopper of the grasshopper swarm in the d th dimension, ub_d, lb_d are the upper bound and the lower bound of the d th dimension in the *i*th grasshopper, $\hat{T}_d$ is the *d*th dimension of the optimal grasshopper. $d_{ij} = \left|x_j^d - x_i^d\right|$ denotes the distance between the *i*th grasshopper and the *j*th grasshopper in the d th dimension. $\frac{x_j - x_i}{d_{ij}}$ is a unit vector from the *i*th grasshopper to the *j*th grasshopper.

$$c = c_{\max} - t\frac{c_{\max} - c_{\min}}{T}, \qquad (2)$$

where $c_{\max}, c_{\min}$ are the maximum value and the minimum value of c, respectively, t denotes the current iteration, and T is the maximum number of iterations. In GOA, $c_{\max} = 1, c_{\min} = 0.000001$ are selected. The coefficient c is used for global exploration and local development of the balance algorithm. The coefficient c decreases the search range of the individual as the number of iterations increases, and is used to control the exploration and development of the algorithm; the coefficient c on the inner side is used to control the attraction zone, comfort zone, and repulsion zone among locusts. And

$$s(r) = fe^{-\frac{r}{l}} - e^{-r}. \qquad (3)$$

Equation (3) is the function of the interaction force between locusts and other grasshoppers. When $s(r) > 0$, the value range of r is called the attraction zone. At this time, the locusts attract each other. Citation; when $s(r) < 0$, the value range of r is

called the repelling zone, and the locusts repel each other; when $s(r)=0$, it is neither attractive nor repulsive, and the value of r is called the comfort zone. In addition, f and l are the attracting strength parameter and the attracting scale parameter, value $f=0, l=1.5$.

From the above analysis, it can be seen that the basic implementation steps of the GOA algorithm are as follows:

*Step*1: Initialize the population size N, the parameters $c_{\max}, c_{\min}$ and the maximum number of iterations $T_{\max}$, initialize the population position, and calculate the fitness value of each grasshopper, and select the optimal value as the target position.

*Step*2: Enter the main loop, and update the parameter c according to formula (2).

*Step*3: According to formula (1) update the individual position of the grasshopper and calculate each grasshopper.

*Step*4: Judge whether the conditions for stopping the loop are satisfied. If it is satisfied, the algorithm will jump out of the loop and return to the target value; otherwise, the algorithm will repeat Step 2 and Step 3.

This article updates the GOA algorithm and uses the updated GOA algorithm to optimize the parameters of VMD.

2.2 Variational Mode Decomposition

VMD proposed in 2014 is an adaptive modal decomposition algorithm, which can make the signal decomposition problem be transformed into a variational problem[9]. Thus the variational problem is obtained as follows:

$$\begin{cases} \min\limits_{\{u_k\},\{w_k\}} \left\{ \sum_{k=1}^{K} \left\| \partial_t \left[\left(\delta(t) + \frac{j}{\pi t} \right) * u_k(t) \right] e^{-jwkt} \right\|_2^2 \right\} \\ s.t. \sum_{k=1}^{K} u_k = x(t) \end{cases}. \tag{4}$$

In equation (4), the original vibration signal $x(t)$ is the accumulation of each IMF obtained by decomposition; $\{u_k\}=\{u_1,u_2,\cdots,u_K\}$ refers to the modal components obtained after the original signal is decomposed; $\{w_k\}=\{w_1,w_2,\cdots,w_K\}$ represents the center frequency corresponding to each IMF obtained by decomposition; ∂_t is the partial derivative of t; $\delta(t)$ is the impulse function.

To obtain the optimal solution to the variational problem, the Lagrange operator $\lambda(t)$ and the quadratic penalty factor α are introduced to make the constrained variational problem be transformed into an unconstrained variational problem, as follows:

$$L(\{u_k\},\{w_k\},\lambda) = \alpha \sum_{k=1}^{K} \left\| \partial_t \left[\left(\delta(t) + \frac{j}{\pi t} \right) * u_k(t) \right] e^{-jwkt} \right\|_2^2 + \left\| x(t) - \sum_{k=1}^{K} u_k(t) \right\|_2^2 + \left\langle \lambda(t), x(t) - \sum_{k=1}^{K} u_k(t) \right\rangle, \tag{5}$$

where $\lambda(t)$ is the Lagrangian multiplier; α is the secondary penalty factor. $\langle \hat{u}_k^{n+1} \rangle, \langle \hat{w}_k^{n+1} \rangle, \hat{\lambda}(t)$ are iteratively updated by the alternating direction multiplier algorithm. Then the "saddle point" of equation (5) can be obtained, that is, the optimal solution of equation (4). In the following, we will use the improved GOA algorithm to optimize the parameters of VMD and find the best decomposition result to facilitate subsequent operations.

2.3 Compressed Sensing

CS is a process of downsampling and decoding the known signal with sparsity[22]. The effective signal is sparse in the sparse domain, but the noise signal is not sparse. Therefore, CS can be utilized to separate the effective signal from the noise.

The basic idea of CS is the following: If the sparsity of an unknown signal is K or is transformed into K spares by a sparse basis, then based on K spares, combined with non-linear transformation, the original signal can be accurately reconstructed. The signal x can be sparsely expressed as a linear combination of the standard orthogonal basis $\Psi=[\phi_1,\phi_2,\cdots,\phi_N]$ as follows:

$$x = \sum_{k=1}^{K} \phi_k \theta_k, \tag{6}$$

where θ_k is the sparse vector of signal x, and the sparsity is k. The smaller the k is, the higher the sparsity is. The signal can be reconstructed accurately until the observation matrix is used to make the signal with the sparse expression be reduced the dimension linearly for projection. The sparseness of the signal is determined by the sparse coefficients θ, so a $M \times N$ measurement matrix is selected to perform a linear transformation on the signal to obtain $y=\Phi x$. The signal x is measured and then the measured value $y \in R^M$ is obtained. Thus

$$y = \Phi x = \Phi \Psi \theta = T\theta, \tag{7}$$

where $T=\Phi\Psi$ is the sensor matrix and θ is the sparse coefficient vector to be solved. Ψ is the orthogonal basis matrix. If the matrix T meets the Restricted Isometry Property (RIP) criterion, K sparse can obtain an optimal solution from the M measured value y. The problem of solving θ by the observation matrix y can be transformed into an optimization problem in the l_0 norm, as follows:

$$\hat{\theta} = \arg\min \|\theta\|_0, s.t. T\theta = y, \tag{8}$$

where $\|\theta\|_0$ is the l_0 norm of θ. The convex relaxation algorithm, the greedy algorithm and the combinatorial optimization algorithm are usually employed to solve Eq.(8). The classical sparse transform methods include discrete cosine transform [23], discrete Fourier transform [24], discrete wavelet transform [25], and other transforms.

In this paper, we choose CS to perform downsampling on the IMF components with the small correlation coefficients obtained by VMD, and the sparse vector θ is obtained. There are two main ways to obtain the measurement matrix: one is to construct it according to the signal characteristics, and the other is to select an existing matrix, such as a random Gaussian matrix. Discrete cosine transform and fast Fourier transform are used to be the sparse basis, Gaussian random matrix and partial Hadamard matrix are chosen to be the measurement matrix, and the orthogonal matching pursuit algorithm is used

to perform the reconstruction. In addition, recent research have shown that the amplified noise signal in the process of random measurement leads to the reduction of the signal-to-noise ratio and the noise folding emerged. Based on this, WT is used to filter the sparse vector θ for reducing the noise folding.

2.4 Wavelet Threshold filtering method

WT filtering method is that the threshold function is used to quantize the decomposed coefficients and then the denoised signal is obtained by the signal reconstruction. There are the common threshold functions, such as hard threshold, soft threshold, Stein Unbiased Risk threshold, heuristic threshold, and soft hard threshold tradeoff.

The data-driven threshold proposed by Donoho [26] widely used at present is defined as follows:

$$T_i = \frac{median\{|\gamma_i|\}}{0.6745}\sqrt{2\log N}, (i = 1,2,\cdots,K), \quad (9)$$

where γ_i is the *i*th IMF component, the *median* is the median function, T_i is the threshold value of the *i*th reconstruction coefficient θ_i which is the *i*th sparse coefficient of the sparse vector θ obtained by the CS algorithm. The wavelet obtained by soft threshold estimation has good sparse continuity and can not produce additional impact. Therefore soft threshold denoising is adopted in this paper, whose expression is as follows:

$$\theta_{i,new} = \begin{cases} \mathrm{sgn}(\theta_i)\cdot(|\theta_i - T|) & |\theta_i| \geq T \\ 0 & |\theta_i| < T \end{cases}, (i = 1,2,\cdots K) \quad . \quad (10)$$

3. The Proposed Denoising Algorithm

3.1 Improved Grasshopper Optimization Algorithm

In the GOA, the position of the grasshoppers is updated by the optimal grasshopper, the current grasshopper, and the other grasshoppers. And the convergence speed of GOA is slow and easy to fall into the local optimal grasshopper. To overcome this disadvantages of GOA, Levy flight and Nonlinear Weight are employed to improve GOA in this paper to obtain the improved GOA, written as IGOA. Levy flight makes individuals conducive to jumping out of the local optimum and finding out the global optimum. Nonlinear weight makes GOA converge to the current local optimum quickly. Levy flight [29] is a method to provide random factors, which are distributed as follows:

$$Levy \sim u = t^{-\lambda}, 1 < \lambda \leq 3.. \quad (11)$$

The nonlinear weight c is taken to be the sigmoid function [30] as follows:

$$c = \frac{1}{1+1.5e^{\frac{10p}{Max\_iter}-5}} - 0.1r, \quad (12)$$

where r is a random number between 0 and 1, and p is the current number of iterations, which makes the algorithm decrease slowly in the early stage and converge rapidly in the later stage. The updated position of the grasshopper is as follows:

$$X_i^d = c\sum_{j=1, j\neq i}^{N} c\frac{ub_d - lb_d}{2} s\left(\left|x_j^d - x_i^d\right|\right)\frac{x_j - x_i}{d_{ij}} + \hat{T}_d + r \times levy(\dim), \quad (13)$$

where $ub_d, lb_d, s(d_{ij}), \hat{T}_d$ are similar to the representation in Subsection 2.1.

Different from GOA, the parameter c in IGOA is used to be equation (12) and the updated position of the grasshopper in IGOA is used to be equation (13). And the number of the terms in equation (13) is more than that in equation (1) and this term is related to Levy fight. The pseudo-code of the IGOA algorithm is shown in Figure 1.

Initialize cmax,cmin, and the population size N, spatial dimension dim
Initialize maximum number of iterations and the swarm X_i(i=1,2,…,N)
Calculate the fitness of each search agent
T=the best search algent
***while** (l<maximum number of iterations)*
Update c using Equation (12)
***For** each search agent*
Normalize the distances between grasshoppers
Update the position of the current search agent by Eq.(13)
Bring the current search agent back if it goes outside the boundaries
end for
Update T if there is a better search algent
l=l+1
end while
Return T

Figure 1. Pseudo codes of the IGOA algorithm.

3.2 The joint denoising algorithm IGOA-VMD-CS-WT

Two parameters of VMD (the number *K* and the penalty factor α of IMFs) need to be set up in advance, which causes the signal cannot be decomposed adaptively by VMD. Given the noise folding phenomenon of CS in the case of a low signal-to-noise ratio, WT is used to process the sparse coefficients after sparse representation of CS to make them more sparse, which reduces the noise overlap phenomenon.

Based on the above analysis, a joint denoising method based on the VMD optimized by IGOA, CS, and WT is proposed in this paper, named by IGOA-VMD-CS-WT, where PSE [27-28] is adopted to be the fitness function.

The concrete steps of IGOA-VMD-CS-WT are as follows:

Step1. Obtain the main frequency f_0 of the noisy signal by Fourier transform. The parameters of VMD are optimized by IGOA to adaptively select the number K of IMFs and the penalty factor α .

Step2. According to the number K of IMFs and the penalty factor α obtained from Step1, the original noisy signal is decomposed by VMD and the K IMF components are retained.

Step3. Calculate the cross-correlation coefficients and center frequency between each IMF component and the

original noisy signal. Based on the cross-correlation value of each IMF component, and the absolute deviation value between the dominant frequency and the center frequency, the bound component is found to distinguish the effective components from the noise components. The effective IMF component is retained directly.

Step4. The noise IMF components processed by downsampling are sparsely expressed. Thus the sparse coefficients $\theta=\{\theta_1,\theta_2,\cdots,\theta_p\}$ are obtained, where p represents the number of noise IMF components, and then WT is used to filter the sparse coefficient θ to get the new sparse coefficients $\theta_{new}=\{\theta_{1,new},\theta_{2,new},\cdots,\theta_{p,new}\}$. Finally, the Orthogonal Matching Pursuit algorithm is used to reconstruct the sparse coefficients to get a denoised noise component.

Step5. The effective components and the denoised noise components are reconstructed to obtain the denoised signal of the original noisy signal.

The flowchart of IGOA-VMD-CS-WT is shown in Figure 2.

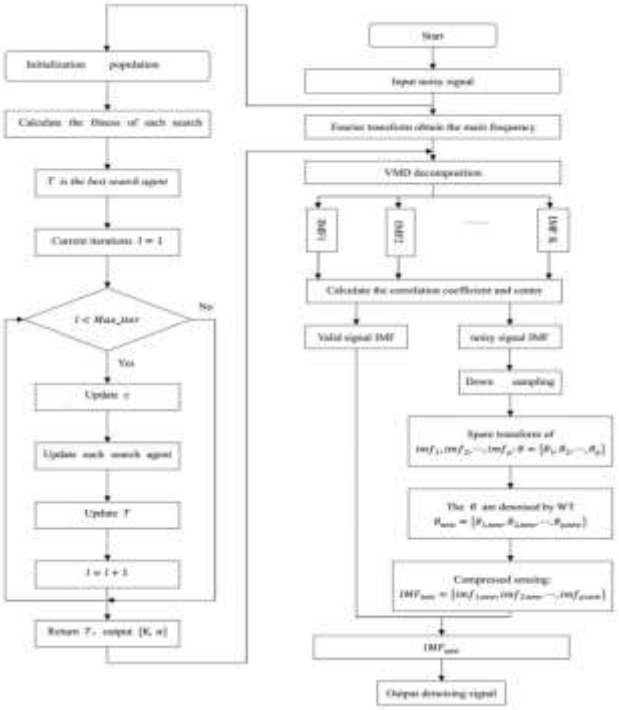

Figure 2. Flowchart of IGOA-VMD-CS-WT

In figure 2, the calculation of fitness value of every agent in the part of VMD optimized by IGOA is as follows:

Every agent in the population is composed of two parameters: the number K and the penalty factor α of IMFs. For every agent, the reconstructed signal of the input noisy signal is obtained by VMD. PSE is calcuated to be fitness value of every agent by the reconstructed signal and the input noisy signal.

4. Simulation Experiments

4.1 Simulation signal

In this paper, the simulation signal is obtained from two sinusoidal signals for performing the denoising performance of the IGOA-VMD-CS-WT. By considering the dynamic changes in the marine environment, the known Gaussian white noise under the different decibels is added to the simulation signal to simulate the noisy signal received by the MEMS vector hydrophone.

The simulation signals are as follows:

$$\begin{cases} y_1(t)=\sin\left(2\times\pi\times400\times t\right)+n(t) \\ y_2(t)=\sin\left(2\times\pi\times200\times t\right)+n(t) \\ y(t)=y_1(t)+y_2(t) \end{cases} \tag{14}$$

where 200 and 400 represent the frequencies of two sinusoidal signals, respectively, and $n(t)$ is the Gaussian white noise with the different decibels.

In this paper, we take the signal-to-noise ratio (*SNR*)

$$SNR=10\log\left(\frac{\sum_{n=1}^{N}x^2(n)}{\sum_{n=1}^{N}\left[x(n)-x'(n)\right]^2}\right) \tag{15}$$

and the root mean square error (*RMSE*)

$$RMSE=\sqrt{\frac{1}{N}\sum_{n=1}^{N}\left[x(n)-x'(n)\right]^2} \tag{16}$$

to be the performance indicators of denoising, where N is the number of snapshots, and $x'(n)$ and $x(n)$ are the denoised signal and the original signal, respectively.

4.2 Denoising of the simulation signal by IGOA-VMD-CS-WT

Due to the limited space, we take the noisy signal with the noisy level at 10dB processed by IGOA-VMD-CS-WT for example in this paper. Figure 3(a) shows the noisy signal with the noisy level at 10dB. Then Fourier transform is performed on the noisy signal and the corresponding frequency spectrum is obtained, shown in Figure 3(b) and its main frequency f_0 is obtained further.

The IGOA is used to optimize two parameters K and α of VMD and the selected K and α are adaptive. Here, the noisy simulated signal is decomposed into 7 IMF components by the optimized VMD. These IMF components and their corresponding spectra are shown in Figure 4. Table 1 shows the cross-correlation coefficients between every IMF component and the noisy simulation signal.

From Figure 4, it can be observed that the energies of IMF1 and IMF2 are the highest, which are the closest to 200Hz and 400Hz, respectively. From Table 1, we can see that the correlation coefficients of IMF1 and IMF2 are the highest. Therefore, IMF1 and IMF2 are regarded to be effective signal components. The other components IMF3-IMF7 with the low correlation coefficients are regarded to be the noise signal components.

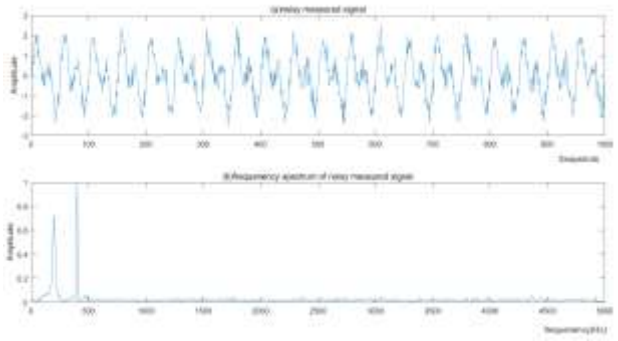

Figure 3. Noisy signal and its corresponding frequency spectrum.

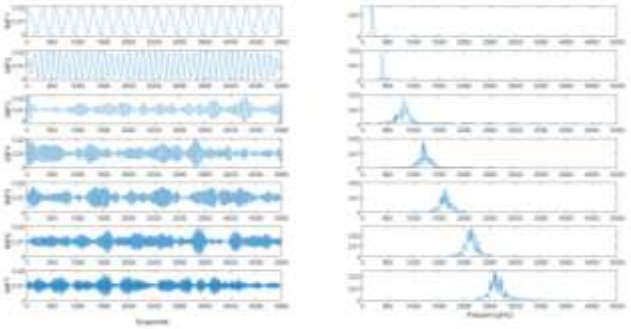

Figure 4. The IMF components and their corresponding spectra obtained by the optimized VMD

For the noise IMF components, CS is utilized to perform denoising. Firstly, 10% of every noise IMF component is selected to perform downsampling. Secondly, the orthogonal basis matrix and measurement matrix are constructed, and the sparse coefficients $\theta = \{\theta_1, \theta_2, \cdots, \theta_p\}$, where p is the number of IMF noise components, are obtained by the sparse representation of the downsampled signal. Thirdly, the WT proposed in this paper is used to process the sparse coefficients, and the new sparse coefficients $\theta_{new} = \{\theta_{1,new}, \theta_{2,new}, \cdots, \theta_{p,new}\}$ are obtained. Finally, the orthogonal pursuit matching algorithm is used to reconstruct $\theta_{new} = \{\theta_{1,new}, \theta_{2,new}, \cdots, \theta_{p,new}\}$, and then the effective IMF components and the denoised noise components are reconstructed to obtain the denoised signal of the original noisy signal. Table 2 shows the signal sparsity and the best sparsity by CS.

4.3 Experimental results

- Comparison of Denoised Effects

In this paper, the joint denoising algorithm IGOA-VMD-CS-WT proposed is the combination of VMD optimized by IGOA, CS, and WT. To verify the effectiveness of the IGOA-VMD-CS-WT, we employ VMD, VMD-CS, VMD-WT, VMD-CS-WT, GOA-VMD-CS, GOA-VMD-WT and IGOA -VMD-WT for comparison with IGOA-VMD-CS-WT on the same noisy signal.

Figure 5 shows the comparisons between the original signal without signal and the denoised signals of the noisy signal with 10 dB Gaussian white noise obtained by these 8 compared algorithms, respectively. Observed in Figure 5, the denoised effects of these 8 compared algorithms are all better, the sharp burrs of the signal are all eliminated, the waveforms are allsmoother as a whole, there are almost no distortion phenomenons, and the edges of the denoisied signal by these 8 compared algorithms have the worse denoised effects except Figure 4(h). The compared results show that the comparison, IGOA-VMD-CS-WT can be used to perform the denoising of the noisy signal, especially to improve the denoising of the edge signal of the noisy signal.

Figure 6 shows the comparisons between the original signal without noise and the denoised signals of the noisy signal with -5 dB Gaussian white noise obtained by these 8 compared algorithms, respectively.

Observed in Figure 6, the denoised signals by VMD-CS and GOA-VMD-CS are not smooth as a whole and there is noise folding, while the waveforms of the denoised signed by VMD, VMD-WT, VMD-CS-WT, GOA-VMD-WT, IGOA-VMD-WT, and IGOA-VMD-CS-WT are all relatively smoother. And owing to WT introduced, the noise folding phenomena are improved. Especially, the denoised signal by IGOA-VMD-CS-WT has the best fitting effect with the original signal without noise.

Based on the above analyses, the compared results show that the denoised effect of IGOA-VMD-CS-WT is better than other methods.

- **Comparison of Denoised Performance Indicators**

The noisy signals with five different decibel Gaussian noises, 15dB, 10dB, 5dB, 0dB, and -5dB, are used to perform denoising by the 8 algorithms: VMD, VMD-CS, VMD-WT, VMD-CS-WT, GOA-VMD-CS, GOA-VMD-WT, IGOA-VMD-WT, and IGOA-VMD-CS-WT, respectively. The *SNR*s and *RMSE*s obtained by these 8 algorithms are shown in

Table 3, where the first column represents the decibel of Gaussian white noise decibels added to the original signal.

Observed from Table 3, the *SNR*s obtained by IGOA-VMD-CS-WT are all the maximum among these 8 algorithms, which are 23.6105 for 15dB, 19.7220 for 10dB, 15.9566 for 5dB, 12.5489 for 0dB, and 9.2686 for -5dB, respectively, and the *RMSE*s obtained by IGOA-VMD -CS-WT are all the minimum among these 8 algorithms,

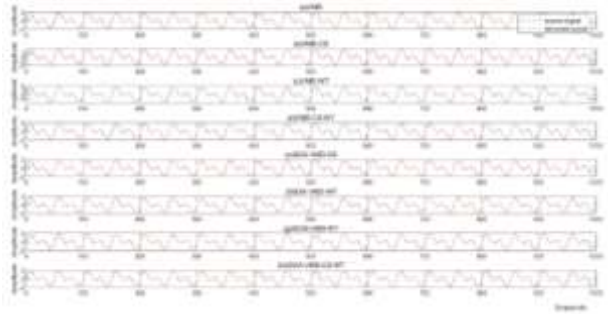

Figure 5. Denoised Effects of the noisy signal with 10dB Gaussian white noise

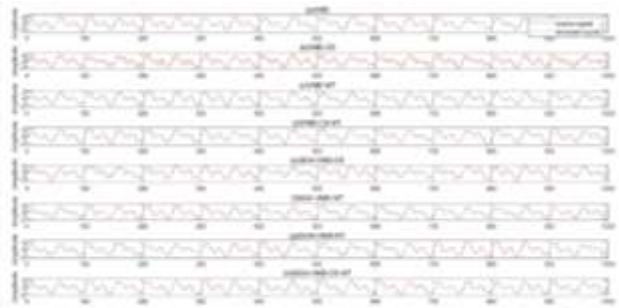

Figure 6. Denoised Effects of the noisy signal with -5dB Gaussian white noise

Table 1. Correlation Coefficients between each IMF Component and the noisy simulation signal.

IMF component	IMF1	IMF2	IMF3	IMF4	IMF5	IMF6	IMF7
Correlation Coefficients	0.6884	0.6737	0.1211	0.1017	0.0981	0.0961	0.0973

Table 2. Signal Sparsity and the Optimal Sparsity

Noise IMF Component	IMF3	IMF4	IMF5	IMF6	IMF7
Signal Sparsity	53	47	52	46	42
Optimal Sparsity	2	2	2	4	1

Table 3. The *SNRs* and *RMSEs* obtained by these 8 algorithms

dB	Performance indicator	VMD	VMD-CS	VMD-WT	VMD-CS-WT	GOA-VMD-CS	GOA-VMD-WT	IGOA-VMD-WT	IGOA-VMD-CS-WT
15dB	SNR	16.1697	17.7802	21.6527	22.3275	21.0024	22.1576	22.9151	**23.6105**
	RMSE	0.1554	0.1291	0.0827	0.0766	0.0904	0.0780	0.0710	**0.0660**
10dB	SNR	15.7538	16.1507	18.4869	18.6940	17.2304	18.6400	19.1025	**19.7220**
	RMSE	0.1630	0.1558	0.1191	0.1164	0.1376	0.1172	0.1110	**0.1041**
5dB	SNR	13.8800	13.2914	14.6015	15.7434	13.4869	15.8678	15.9022	**15.9566**
	RMSE	0.2023	0.2437	0.1862	0.1641	0.2117	0.1611	0.1603	**0.1593**
0dB	SNR	10.2194	9.0332	11.1042	11.6070	9.1175	12.0430	12.3616	**12.5489**
	RMSE	0.3038	0.3554	0.2785	0.2628	0.3501	0.2504	0.2410	**0.2359**
-5dB	SNR	6.8692	4.4314	6.9463	7.2939	4.6269	7.3714	7.6339	**9.2686**
	RMSE	0.4535	0.6006	0.4495	0.4321	0.5870	0.4280	0.4154	**0.3440**

which are 0.0660 for 15dB, 0.1041 for 10dB, 0.1593 for 5dB, 0.2359 for 0dB and 0.3440 for -5dB. Thus the denoised effect of IGOA-VMD-CS-WT is significantly better than those of the other compared algorithms under the different decibel noises. That is, IGOA-VMD-CS-WT is superior to VMD, VMD-CS, VMD-WT, VMD-CS-WT, GOA-VMD -CS, GOA-VMD-WT, IGOA-VMD-WT. In addition, the denoised effect of IGOA-VMD-WT is slightly better than GOA-VMD-WT, which indicates that the improved GOA improves the SNR and RMSE and further that IGOA is better than GOA.

Based on the comparisons of denoised results and the performance indicators, when the noise level is low, the simple CS is used to perform denoising, and then there exist noise folding phenomena, but once the WT denoising is introduced, the noise folding phenomena are improved and the denoised signal is better, the SNRs are higher. All of these further demonstrate that the proposed IGOA-VMD-WT algorithm has a better-denoised effect on the noisy signal with different decibel noise and the baseline drift removal, outperforms VMD, VMD-CS, VMD-WT, VMD-CS-WT, GOA-VMD-CS, GOA-VMD-WT, IGOA-VMD-WT.

5. Lake Trial Experiments

The measured data used in this paper are derived from fenji experiments conducted by the North University of China in 2011 and 2014 in fenhe, respectively.

5.1 Experiment 1: The measured data from the fenji331Hz data packet tested in 2011.

In this experiment, the vector hydrophone with 5-element linear array was fixed on the shore and the transducer was placed on the tugboat. The anchor was dropped at the different positions, and then the measured data was collected by the transducers. The sound source with a transmitting signal frequency of 331Hz is 6 meters far away from the vector hydrophone with a sampling frequency of 10kHz. The data with the snapshots1000 arbitrarily intercepted from the measured data of five road array signals are regarded to

be the noisy data for performing the signal denoising.

Figure 7(a)(b)-Figure11(a)(b) show the signals of the 1-Road array to the 5-Road array and their corresponding frequency spectra, respectively. And Figure7(c)(d) -Figure11(c)(d) show the denoised signals of 1-Road array to 5-Road array processed by IGOA-VMD-WT and their corresponding frequency spectra.

Observed in Figure 7(a)(b)-Figure11(a)(b), there exists a small amount of noise in 1-Road and 2-Road array signals, while there exist a large amount of noise in 3-Road, 4-Road and 5-Road array signals. Observed in Figure7(c) -Figure11(c), the sharp burrs of the signals have been effectively eliminated, the signal becomes smooth and tidy and the distorted part of the signal is effectively improved. Observed in Figure7(d)-Figure11(d), the energies of the signals are hardly lost and the noises have been eliminated effectively.

5.2 Experiment 2: The measured data from the fenji measured data in 2014.

In this experiment, the MEMS vector hydrophone with 5-element arrays of interval distance of 0.5 meters was placed on the shore, and the transducer was placed on the tugboat. The MEMS vector hydrophone was placed under the water 2 meters and was kept horizontal. Thus the MEMS vector hydrophone could continuously output the sound pressure and the circuit signals. The signal signals with 315Hz, 500Hz, 630Hz, 800Hz, and 1000Hz are obtained by adjusting the transducer, respectively. The data with the snapshots 1000 are arbitrarily intercepted from the different frequency packets to be regarded as noisy signals.

Figure 12(a)(b)-Figure 16(a)(b) show the signals with 315Hz, 500Hz, 630Hz, 800Hz, and 1000Hz and their corresponding frequency spectra, respectively. And Figure7(c)(d)-Figure11(c)(d) show the denoised signals with 315Hz, 500Hz, 630Hz, 800Hz and 1000Hz processed by IGOA-VMD-WT and their corresponding frequency spectra.

Observed in Figure 12 (a)(b)-Figure 14(a)(b), there exists the low-frequency noise in the upper part of the signal and the high-frequency noise in the lower part of the signal, and there exist the serious distortions in the signals. Observed in Figure15(a)(b)-Figure16(a)(b), there exists a slight noise and no serious distortion in the signals, but the waveforms of the signals are not smooth. And the baseline drift removals are improved. Observed in Figure12(c)-Figure16(c), the noises of the noisy measured signals are all eliminated and the waveforms of the denoised measured signals are all well recovered. And there are no distortion phenomena and the basic characteristics of the original signals are all well preserved. Observed in Figure12(b)(d) -Figure16(b)(d), the energies of the signals are also well preserved with no loss.

5.3 Experimental results

Based on the above two experiments, the IGOA-VMD-CS -WT algorithm proposed in this paper can effectively eliminate the noise, better recover the basic characteristics of the signal, and improve the baseline drift removal. Therefore, the IGOA-VMD-WT algorithm proposed in this paper is effective and suitable for signal denoising. At the same time, the IGOA-VMD-WT algorithm proposed in this paper gives support for the next location, classification, and recognition of the signal.

6. Conclusion

In this paper, IGOA is used to optimize the parameters of VMD to establish the hybrid algorithm IGOA-VMD. Based on the combination of IGOA-VMD, CS, and WT, the joint signal denoising algorithm IGOA-VMD-CS-WT of MEMS vector hydrophone is proposed. The simulation experiments show that the proposed IGOA-VMD-CS-WT can effectively eliminate the noises from the noisy signals, and has the minimum *RMSEs* and the maximum *SNRs*. And the compared results show that the proposed IGOA-VMD-CS-WT outperforms the other compared algorithms and weakens the noise folding. Further, the proposed IGOA-VMD-CS-WT is applied to perform the denoising of the measured signals derived from fenji experiments conducted by the North University of China in 2011 and 2014 in fenhe. And the denoised results show that the proposed IGOA-VMD-CS-WT can effectively eliminate the noise of the measured signals and improve the baseline drift removal.

In addition, the IGOA is obtained from GOA by introducing the Levy flight and the nonlinear weight. But the selections of different nonlinear weight lead to the different IGOA and the combination of GOA and the other one or two warm intelligence algorithms generates different IGOA. These improved GOAs are combined with VMD, CS, and WT to establish the new joint denoising algorithms. The denoising performance of these algorithms will be verified in the future
and be conducive to the subsequent signal location, classification, and recognition of signals.

Acknowledgment

The authors would like to thank the editors and anonymous reviewers for their valuable comments and suggestions, which greatly improved the presentation of the paper. This work was supported in part by the Fundamental Research Program of Shanxi Province (Grant No. 20210302123019, 202103021224195, 202103021224212, 202103021223189), and by the Shanxi Scholarship Council of China (Grant No. 2020-104,2021-108).

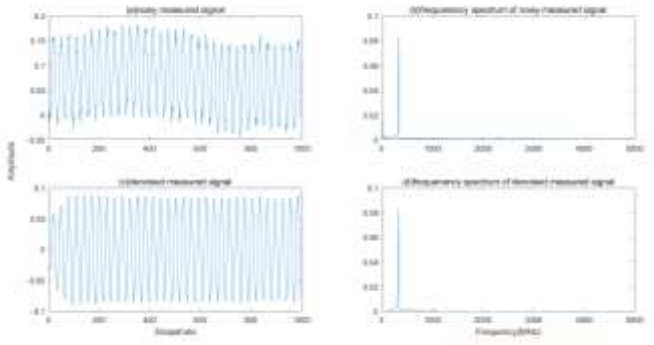

Figure 7. The signal and the denoised signal of 1-Road array signal and their corresponding frequency spectra

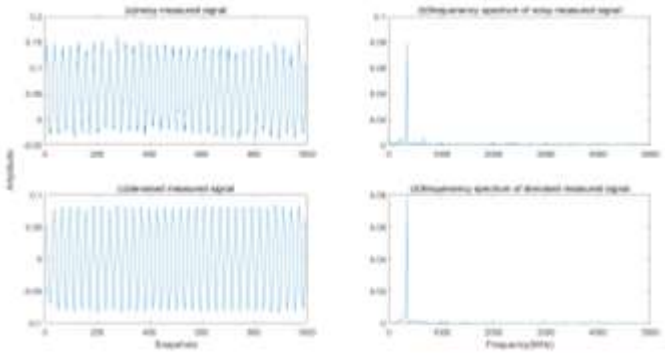

Figure 8. The signal and the denoised signal of 2-Road array signal and their corresponding frequency spectra

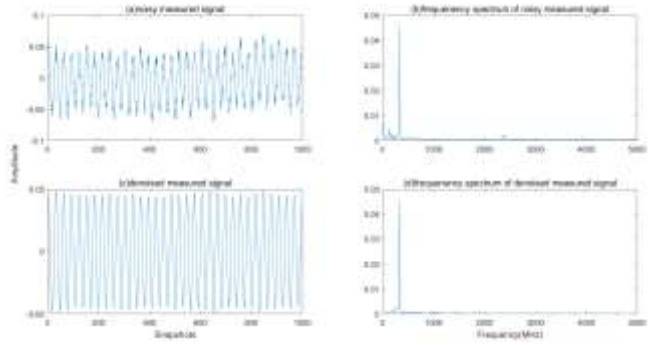

Figure 9. The signal and the denoised signal of 3-Road array signal and their corresponding frequency spectra

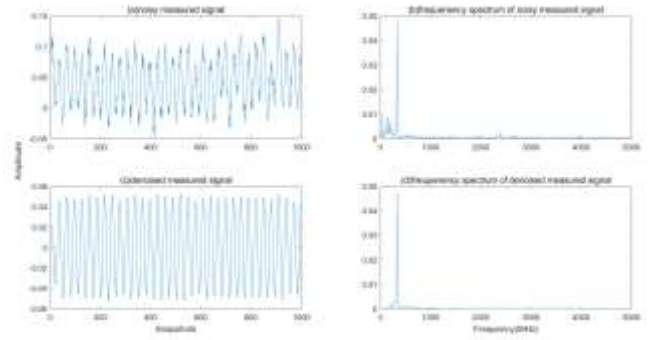

Figure 10. The signal and the denoised signal of 4-Road array signal and their corresponding frequency spectra

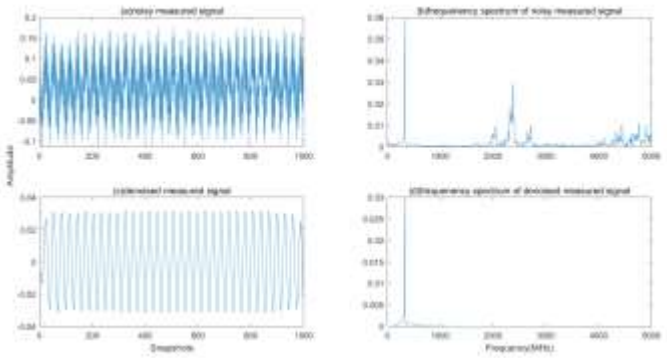

Figure 11. The signal and the denoised signal of 5-Road array signal and their corresponding frequency spectra

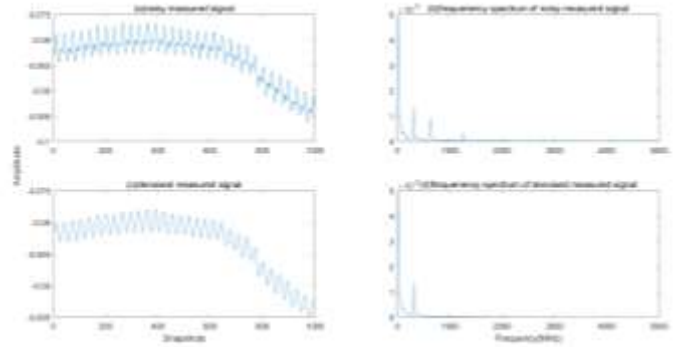

Figure 12. The signal and the denoised signal with 315Hz and their corresponding frequency spectra

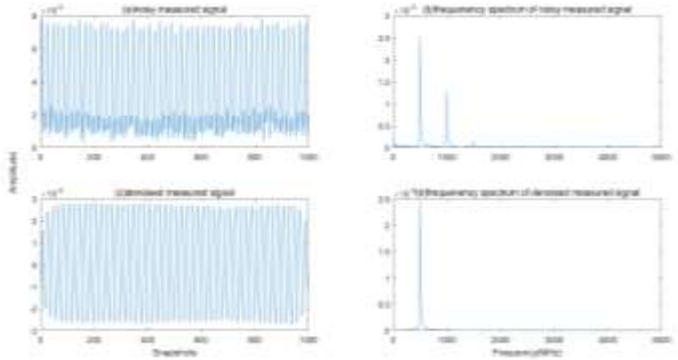

Figure 13. The signal and the denoised signal with 500Hz and their corresponding frequency spectra

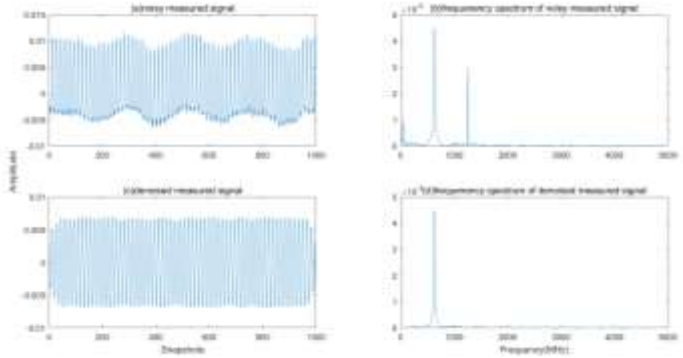

Figure 14. The signal and the denoised signal with 630Hz and their corresponding frequency spectra

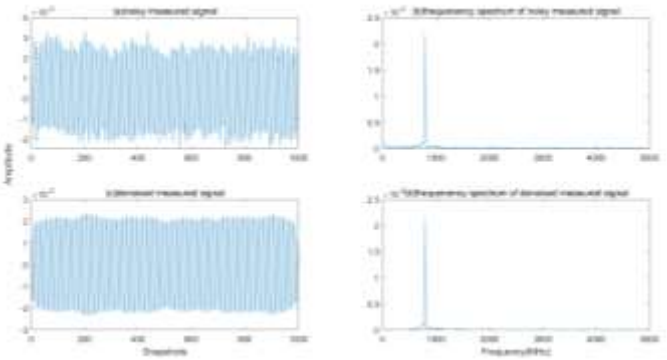

Figure 15. The signal and the denoised signal with 800Hz and their corresponding frequency spectra

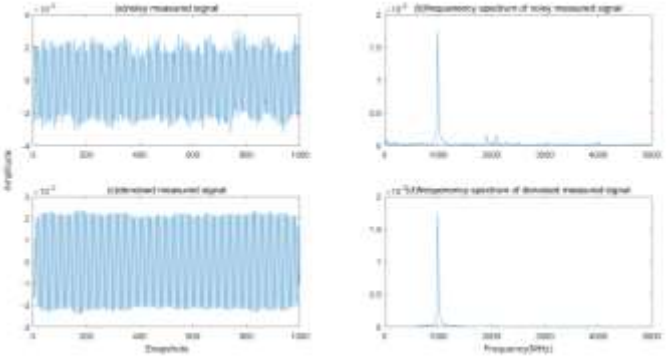

Figure 16. The signal and the denoised signal with 1000Hz and their corresponding frequency spectra

References

[1] C.Y. Xue, S. Chen, W.D. Zhang, B.Z. Zhang, G.J. Zhang, H. Qiao, "Design, fabrication, and preliminary characterization of a novel MEMS bionic vector hydrophone," *Microelectronics Journal*, vol.38, pp. 1021-1026,2007.

[2] B.Z. Zhang, H. Qiao, S. Chen, J. Liu, W.D. Zhang, J.J. Xiong, C.Y. Xue, G.J. Zhang. "Modeling and characterization of a micromachined artificial hair cell vector hydrophone," *Microsystem Technologies-micr-and Nanosystems-Information Storage and Processing Systems*, vol. 14(6), pp. 821-828, 2008.

[3] A. Peyman, K. Zoheir, H. Kourosh, "Design of a MEMS bionic vector hydrophone with piezo-gated MOSFET readout," *Microelectronics Journal*, vol.98, pp. 104748, 2020.

[4] G.J. Zhang, Q.D. Xu, C. Zhang, S. Chen, S. Yang, "Optimization of Shell Packaging for Cilium MEMS Bionic Vector Hydrophone," *Sensors and Actuators A -Physical*, vol.306, pp.111969,2020.

[5] M S S M Basir, R C Ismail, K H Yusof, N I A Katim, M N M Isa, S Z M Naziri," An implementation of Short Time Fourier Transform for Harmonic Signal Detection," *Journal of Physics: Conference Series*, vol.1755, pp. 012013,2021.

[6] A. Kumar, H. Tomar, V. K. Mehla, R. Komaragiri, M. Kumar," Stationary wavelet transform based ECG signal denoising method," *ISA Transactions*, 2020.

[7] XA.Yan, Y. Liu, Y.D. Xu, M.P. Jia," Multichannel fault diagnosis of wind turbine driving system using multivariate singular spectrum decomposition and improved Kolmogorov complexity," *Renewable Energy*, vol.170, pp. 724-748,2021.

[8] N. E. Huang, Z. Shen, S.R. Long, M.C. Wu, H. H. Shih, Q. A. Zheng, N.C. Yen, C.C. Tung, H.H. Liu," The empirical mode decomposition and the Hilbert spectrum for nonlinear and non-stationary time series analysis," *Proc. R. Soc. Lon.*, vol.454,pp.903-995,1998.

[9] K. Dragomiretskiy, D. Zosso, "Variational Mode Decomposition," *IEEE Transactions on Signal Processing*, vol.62(3), pp.531-544,2014.

[10] H.P. Hu, L.M. Zhang, H.C. Yan, Y.P. Bai, P. Wang," Denoising and baseline drift removal method of MEMS hydrophone signal based on VMD and wavelet threshold processing," *IEEE Access*, vol. 7,pp.59913-59922,2019.

[11] F. Javier, "Metaheuristics: from Design to Implementation," *Interfaces*, vol. 42, pp. 414-415, 2012.

[12] A.A. Heidari, S. Mirjalili, H. Faris, I. Aljarah,M. Mafarja, H.L. Chen, "Harris hawks optimization: Algorithm and applications," *Future Generation Computer Systems*, vol. 97, pp.849-872, 2019.

[13] J.R. Koza, "Genetic Programming II. Automatic Discovery of Reusable Subprograms," MIT Press, Cambridge, MA,1992.

[14] J.H. Holl, " Genetic algorithms," *Sci. Amer.*, vol. 267(1), pp. 66-73, 1992.

[15] J. Kennedy, R. Eberhart, "Particle swarm optimization," In *Proc. Int. Conf. Neural Netw., Perth*, *WA, Australia*, Nov./Dec. 1995, pp.1942-1948.

[16] S. Saremi, S. Mirjalili, A. Lewis, "Grasshopper Optimization Algorithm: Theory and application," *Advances in Engineering Software*, vol.105, pp.30-47, 2017.

[17] H.C. Yan, T. Xu, P. Wang, L.M. Zhang, H.P. Hu, Y.P. Bai. MEMS Hydrophone Signal Denoising and Baseline Drift Removal Algorithm Based on Parameter-Optimized Variational Mode Decomposition and Correlation Coefficient. Sensors 2019, 19, 4622.

[18] H.P. Hu, Y. Ao, Y.P. Bai, H.C. Yan, N. Shi."Signal Denoising Based on Wavelet Threshold Denoising and Optimized Variational Mode Decomposition," *Journal of Sensors*, vol. 2021, Article ID 5599096, 2021.

[19] X. Li, L.L. Dong, B. Li, Y.F. Lei, N.W. Xu," Microseismic Signal Denoising via Empirical Mode Decomposition, Compressed Sensing, and Soft-thresholding," *Applied Sciences-Basel*, vol.10(6), pp.2191,2020.

[20] M.M. Sun, Z.C. Li, Z.N. Li, Q.Y. Li, Y.L. Liu, J. Wang, "A noise attenuation method for weak seismic signals based on compressed sensing and CEEMD,". *IEEE Access*, vol. 8, pp.71951-71964,2020.

[21] X.B. Xu, M. Zhang, M.Z. Luo, J. Yang, Q.y. Qu, Z.Y. Tan, H. Yang, "Echo Signal Extraction Based on Improved Singular Spectrum Analysis and Compressed Sensing in Wavelet Domain," *IEEE Access*, vol.7, pp. 67402-67412,2019.

[22] L.J. Yu, X.C. Xie, "Brief Introduction of Compressed Sensing Theory,"*Video Engineering*, vol. 32(12), pp.16-18, 2008.
[23] N N Ahmed, T Natarajan, K R Rao, "Discrete Cosine Transform," *IEEE Transactions on Computers*, vol. C-23(1), pp. 90-93,2006.
[24] LEO I. BLUESTEIN," A linear filtering approach to the computation of discrete Fourier transform," *IEEE Transactions on Audio & Electroacoustics*, vol. AU-18(4), pp.451-455, 1970.
[25] C.L. Chang, B. Girod, "Direction-adaptive discrete wavelet transform for image compression," *IEEE Transactions on Image Processing*, vol. 16, pp. 1289-1302, 2007.
[26] D.L. Donoho, "De-noising by soft-thresholding," *IEEE Transactions on Information Theory*, vol. 41(3), pp. 613-627,2002.
[27] Z.J. Wang, G.F. He, W.H. Du, J. Zhou, X.F. Han, J.T. Wang, H.H. He, X.M. Guo, J.Y. Wang, Y.F. Kou," Application of Parameter Optimized Variational Mode Decomposition Method in Fault Diagnosis of Gearbox," *IEEE Access*, vol.7, pp.44871-44882,2019.
[28] Y.J. Ji, X.B. Wang, Z.B.Liu, Z.H. Yan, L. Jiao, D.Q. Wang, J.Q. Wang, "EEMD-based online milling chatter detection by fractal dimension and power spectral entropy," *International Journal of Advanced Manufacturing Technology*, vol.92(1-4), pp. 1185-1200,2017.
[29] D. Mokeddem, "Parameter Extraction of Solar Photovoltaic Models Using Enhanced Levy Flight Based Grasshopper Optimization Algorithm," *Journal of Electrical Engineering and Technology*,vol.16(1), pp.171-179, 2020.
[30] Y. Ito, "Approximation of functions on a compact set by finite sums of a sigmoid function without scaling," *Neural Networks*, vol.4(6), pp.817-826,1991.

HONGPING HU received a Ph.D. degree from the North University of China, Shanxi, China, in 2009. She is currently a Professor and a master's tutor in the School of Science, North University of China, Shanxi, China. Her research interests include combinatorial mathematics, artificial intelligence, signal processing, and image processing.

Contribution of Individual Authors to the Creation of a Scientific Article (Ghostwriting Policy)

Hongping Hu and Nana Zou have implemented the proposed denoising algorithm of Section III. Nana Zou carried out the simulation and the experiments and wrote the manuscript. And Hongping Hu and Yanping Bai were responsible for revising and giving suggestions.